PCCP

Accepted Manuscript

ROYAL SOCIETY OF CHEMISTRY

www.rsc.org/pccp

Phys. Chem. Chem. Phys.

PERSPECTIVE

Simulations of Molecular Self-Assembled Monolayers on Surfaces: Packing Structures, Formation Processes and Functions Tuned by Intermolecular and Interfacial Interactions

Received 00th January 20xx,
Accepted 00th January 20xx

DOI: 10.1039/x0xx00000x

www.rsc.org/

Jin Wen,[a] Wei Li,[a] Shuang Chen[b] and Jing Ma[a*]

Surfaces modified with functional molecular monolayer are essential for the fabrication of nano-scale electronics or machines with novel physical, chemical, and/or biological properties. Theoretical simulation based on advanced quantum chemical and classical models is at present a necessary tool in the development, design, and understanding of interfacial nanostructure. The nanoscale surface morphology, growth processes, and functions are controlled by not only the electronic structures (molecular energy levels, dipole moments, polarizabilities, and optical properties) of building units but also the subtle balance between intermolecular and interfacial interactions. The switchable surfaces are also constructed by introducing the stimuli-responsive units like azobenzene derivatives. To bridge the gap between experiments and theoretical models, opportunities and challenges for future development of modelling of ferroelectricity, entropy, and chemical reactions of surface-supported monolayers are also addressed. Theoretical simulations will allow us to gain important and detailed information about the structure and dynamics of monolayer modified interfaces, that will inform the rational design and optimization of dynamic interfaces to meet challenges of controlling optical, electrical, and biological functions.

1 Introduction

Molecular self-assembled monolayers (SAMs) are formed spontaneously on a variety of solid surfaces with ordered two-dimensional (2-D) structures and interesting packing patterns.[1–5] Although the thickness of a SAM is just in the nanometer magnitude, a thin layer of orderly arranged molecules can dramatically change the properties of a surface. SAM strategies for modifying various surfaces provide versatile platforms for different applications such as protecting surface, building molecular electronic devices, and fabricating smart surfaces and biosensors.[6] Construction of 2-D molecular nanostructures has been widely applied for the integration of various organic molecules from optical/electric toolbox into devices and for the creation of functional nanomaterials or molecular electronics.[7,8] The functions of SAMs are expanded by introducing the stimuli-responsive units and hence the non-equilibrium dynamic behaviors.[9] With this premise, smart surfaces that have switchable properties have attracted long-term attention in the aspect of molecular machines for the past four decades.[10,11] The surface-mounted monolayers with functional groups present tunable morphology under external stimuli (such as light, electrical potential, thermal and chemical/biochemical changes), leading to potential applications in chemical sensors or biosensors, electronic switches, and optical memories.[12–17] The protein or enzyme toolbox has been recently harnessed for SAM fabrication to regulate the biological activity of artificial tissues or surfaces.[18–22] Those SAM functionalized surfaces can be fabricated by using both bottom-up and top-down technologies with the help of advanced analytical tools.

However, nanoscale control of surface or interface properties is a grand challenge for producing various functional surfaces and nanomaterials at will. The manipulation of nanoscale surface morphology and function requires the precise control over not only the electronic structures (molecular energy levels, dipole moments, polarizabilities, and optical properties) of building units but also the competition between intermolecular and interfacial interactions.

From understanding to rational design of the nanostructures, the computational modelling serves as a powerful tool for bridging the gap between the experiment and theory. Firstly, it is recognized that investigation in the dynamic process of functional monolayers plays an essential role in revealing the mechanism of different energy conversion processes.[23,24] Secondly, different molecules can be tested to find its working performance by computational simulations before they are synthesized. The candidate molecules then will be selected as building blocks of potential functional monolayers to fabricate the 2-D materials and smart surfaces. Thirdly, the observed images from scanning tunnel microscope (STM) or atomic force microscope (AFM) can be rationalized and assigned by detailed packing styles of building units from theoretical simulations.[25–30] The knowledge of some specific and directional intermolecular interactions such as hydrogen bonding between the π-conjugated function units has been widely applied to build various alignment patterns and hence film morphologies on solid surfaces.[25–27]

Due to the complexity of surface models and the competition between intermolecular and interfacial interactions, unfortunately, relatively fewer theoretical studies have been performed on the surface-supported SAMs than those on the isolated molecules in gas phase or solution.[31–34] This perspective will focus on theoretical

[a] Institute of Theoretical and Computational Chemistry, Key Laboratory of Mesoscopic Chemistry of MOE, School of Chemistry and Chemical Engineering, Nanjing University, Nanjing 210093, P. R. China
[b] Kuang Yaming Honors School, Nanjing University, Nanjing, Jiangsu 210023, P. R. China

Electronic Supplementary Information (ESI) available: Computational details, binding energies, dipole moment, and quadruple moments of 5T systems are listed in the Table S1-S4. See DOI: 10.1039/x0xx00000x

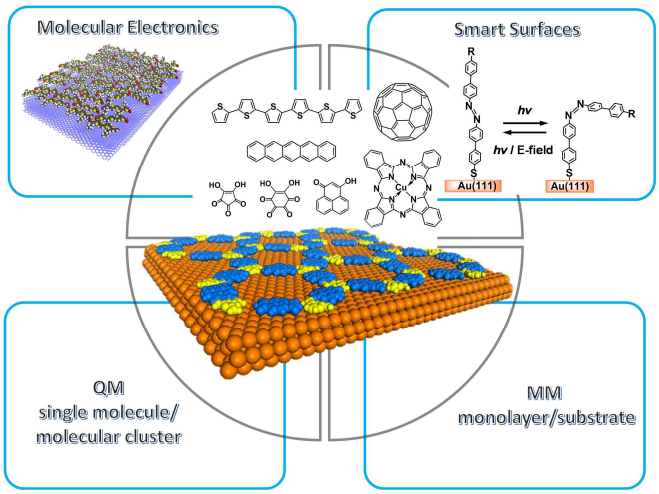

Fig. 1 Establishment of the structure-function relationship of self-assembled monolayers with quantum mechanics (QM) and molecular mechanics (MM) methods.

studies of various SAMs done by our group[29,30,35–38] and some other collaboration groups,[25–28,39,40] which is motivated by experimental advances and observations but aims at gaining deeper understanding of the relationship between the macroscopic properties of materials and electronic structures of building blocks as well as the packing patterns on the surface.

In the screening of candidates of SAM building units from toolbox with the desired functions, a combination strategy of quantum mechanics (QM) and molecular mechanics (MM) is usually employed in the molecular modelling from a single molecule to the molecular aggregates in the molecular monolayers (Fig. 1). Once the physical properties, such as charge, dipole moment, polarizability, optical absorption/emission, and conductivity in the proposed molecule are known by QM, we can modify the functional groups in this molecule to adjust the demanded properties of each building unit. Nevertheless, these predictions are made on the basis of electronic structure of a single isolated molecule or minimum-sized aggregate (e.g., dimer or trimer). To characterize global properties of the whole monolayer on the surface, MM is used to study the interfacial and intermolecular interactions firstly and then their packing morphologies. Good agreements have been achieved between the experimental STM images and the predicted packing structures of various π-conjugated building units, such as oligothiophene (*n*T, *n*=4–6),[30,35] 3,4,9,10-perylenetetracarboxylic dianhydride (PTCDA),[26] and copper(II) phthalocyanine (CuPc)[27,28,39] in 2-D SAMs on the solid surfaces. In this perspective, we will classify the studied building molecules into two classes: the non-polar units (with centrosymmetry) and the polar ones (with nonzero permanent dipole moments). Although the symmetric units like sphere fullerene (C_{60}), rod-like pentacene (Pn), and disc-like metal phthalocyanine (MPc, M=Cu) bear very different topologies from each other, they belong to the first non-polar type, whose packing morphologies are largely controlled by the van der Waals (vdW) interactions. In the present work, we will lay emphasis on the second class with polar building units such as oligothiophenes with n=5 (called 5Ts), 3-hydroxyphenalenone (3-HPLN), and oxocarbon acids, $H_2C_nO_n$, with n = 5 and 6. It will be shown that the dipole-dipole interactions dominate the non-bonded interactions and hence control the packing structure and the physical functions (e.g., ferroelectricity).[40,41]

Traditional force field (also called MM) has been shown its successful applications in simulations of various self-assembly structures on surfaces at the equilibrium stage. However, when the external stimuli were employed, the monolayers were not in their equilibrium state any more. In this case, reactive force field was developed to simulate this non-equilibrium state in the molecular dynamics (MD) runs.[42,43] Being fitted from the diabatic potential energy surfaces for *cis* and *trans* isomers, the alternative *trans*→*cis* and the reverse *cis*→*trans* potentials were applied together with switching functions to model the stimuli-induced collective isomerization process of azobenzene-based SAM on Au (111) surface or in the solution in reactive MD simulations.[36–38,44,45]

The following sections of this perspective will start from the analysis of electronic structure of some widely-used functional units, then we will discuss the driving forces (both interfacial and intermolecular interactions) for these building units to assemble into the ordered functional monolayers on the surfaces, and we will give some examples of functional SAMs with novel ferroelectric or dynamic switching properties in simulations studied by *ab initio* molecular dynamics or traditional and reactive force fields. Some systems we studied have been synthesized before and good agreements between the experiments and simulations were demonstrated, while some of them are predicted to have interesting nanostructures or ferroelectricity by our simulations. Opportunities and challenges for future development of theoretical models to better treat ferroelectricity, entropy, and chemical reactions of surface-supported monolayers are also addressed. In the near future, theoretical designs of novel target units could be extensively used to see whether they are feasible as functional monolayers on the surfaces before the experimental synthesis, which can dramatically reduce the expense on the experimental work. The understanding of the nature of intermolecular interactions between the non-polar or polar groups as well as the interfacial interactions between the building units and the metal or non-metal surfaces is very useful to fabricate 2-D SAMs with various desired morphologies.

2 Building units with interesting electronic structures and functions

Up to now, several kinds of molecules have been used as the functional units in building surface-mounted monolayers, including π-conjugated molecules, functionalized alkyl chains, biomolecules, and polymers. Usually the building units from the experimental tool box are classified according to their functions. For example, nTs, Pn, C_{60}, and CuPc are taken as controlled injection barriers in organic thin-film devices or as the candidates in bulk heterojunction photovoltaic cells. Recently, the application of peptide building units in building various SAMs for the usage of surface biosensors has been continuously heated up. However, such a function-based classification of building blocks cannot be directly correlated with the intermolecular interactions between the function units, which are very important to control the packing styles on surfaces in practice. Instead, according to the intrinsic electronic structures, we classify the typical function units into two groups, non-polar versus polar units. The SAMs formed with the non-polar units such as 4T, Pn, and CuPc were extensively studied both experimentally and theoretically.[25–28,30,35,39] It will be shown that the self-assembled molecular nanostructures on surfaces are mainly determined by the vdW interactions between each non-polar unit. In some cases, the directional hydrogen bonding interactions were also employed to

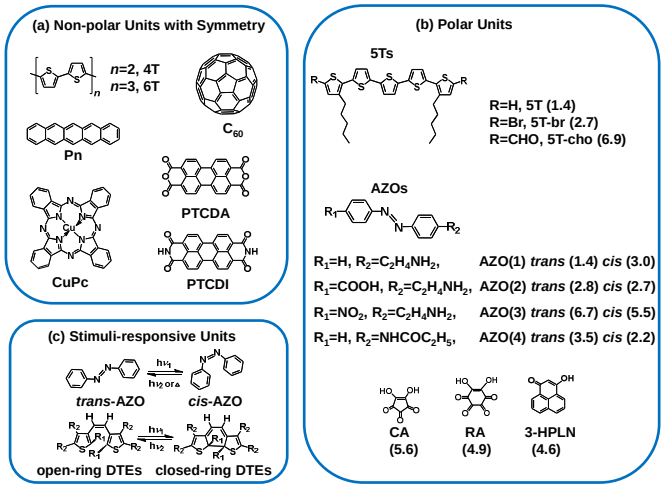

Fig. 2 Illustration of the toolbox of (a) non-polar and (b) polar building units or (c) stimuli-responsive units. For the polar units, the magnitude of the dipole moment (in units of Debye, 5Ts at M06-2X/6-31G* level, AZOs at CAM-B3LYP/6-31+g** level, and CA/RA/3-HPLN at MP2/6-31+G* level) of each conformation is given in parentheses.

tune the packing orientations of building blocks.[26,29]

In contrast, the applications of polar units with non-negligible dipole moments to build the functionalized SAMs are much less. However, the response of the polar unit to the external stimuli (such as light irradiation or the electric field) and the collective polarization effects add many novel optical-electric or ferroelectricity properties.

In such cases, electrostatic interactions dominate the packing structures and functions of SAMs rather than vdW interactions. In order to increase the polarity of the building units, the asymmetric substitutions at two edges of the π-conjugated systems with donor–π–acceptor (D–π–A) structure, such as the functionalized azobenzenes (AZOs) and 5Ts in Fig. 2b are often used to synthesis promising candidates for molecular electronic devices.[46–49] The interesting optical or electricity functions stem from the intra- or inter-molecular charge transfer in these push-pull molecules and high polarizability under light irradiation or electric field.[50–52] The polar units of CA, RA, and 3-HPLN with the dipole moment of about 5 Debye are also used in fabricating the organic ferroelectric monolayers and bilayers on metal surfaces.[40,41]

The dynamic stimuli-responsive units constitute the third class, which may overlap with the above mentioned polar and non-polar units. The external stimuli include the energy-based triggers (like light, electric field, and temperature) and the chemical based changes (such as pH, ionic strength, solvents, and complexations with metal ions or biomolecules). The applications of photochromic complexes have been reported as UV-Vis responsive units in data-storage devices[53] and optical switches,[54] in which the photo-induced isomerization reactions occur in their photo-responsive parts. As a photo-responsive molecule, AZO with a high trans-cis conversion rate for its configuration rearrangement is used extensively in molecular switches. In addition, it was found that AZO derivative could form SAM on TiO_2 surface, which was used as a dye in the application of dye sensitized solar cells.[55] Moreover, when the AZO monolayer was contacted with a SAM modified Hg droplet, it could be used as a molecular lifting-cargo, whose switching process was simulated to give microscopic details of the switching dynamics.[36,56] Dithienylethene (DTE) derivatives undergo a cyclization/cycloreversion reaction between their open-ring and closed-ring isomers (Fig. 2c). Therefore, they have potential applications in optical memories and switches.[57] Recently, spiropyrans and spirooxazines have been studied in three-dimensional optical memory and photo switches of protein because of their reversible colour change under UV light of different wavelengths.[58–60] Another kind of UV-VIS responsive unit, quinones, such as phenoxynaphthacene quinone has photo isomerization between the redox-active trans-state and the redox-inactive "ana"-state,[11] which can be operated by a mixture of photonic and electric stimuli. Once these units are assembled into smart monolayers on substrates, the film morphologies and functions are tuneable between the different ON and OFF states under the radiation. It will be addressed in section 4 that simulations of the collective switching processes of those photochromic compounds such as AZOs and DTEs face big challenges in using traditional molecular dynamics models and new reactive models were developed for such surface switches.

3 Packing structures controlled by intermolecular and interfacial interactions

The engineering of the architecture and patterns of SAM is a key to achieve some specific electronic or optical functions. We can tune the pattern of SAM by adjusting the compatibility of interfacial and intermolecular interactions. A successful simulation of packing structures relies on an accurate description of electronic structures and the intermolecular interactions of the building units in monolayers on the surfaces. The binding energy, E_b, between the surface and monolayer and the interaction energy within the monolayer can be calculated by QM or MM methods, depending on the accuracy of computational model.

3.1 Interfacial interactions

A cluster model with truncated surface could be used to study the interfacial interaction between a single molecule and the surface by QM calculations, but it would be expensive to simulate the dense-packed structure. Another type of surface model, a slab model with periodic boundary conditions (PBC) in three dimensions is widely used to simulate the deposition of molecular monolayer on the surface. If the monolayer is constructed by heterogeneous molecular structure, which will require a much larger slab model, the dynamic simulations are too time-consuming by the QM calculation. In this case, the MM method could be employed in the MD simulations when the force field parameters are fitted or validated by QM results of the binding energies and optimized geometries.

The π-π and vdW interactions. When compared to QM binding energies, some conventional force fields are shown to be good enough to describe the π-π interactions between the π-conjugated molecules and highly oriented pyrolytic graphite (HOPG) substrates (Fig. 3a). The weak interfacial interactions between the inert graphite and the adsorbed molecules are usually too weak to bind the organic molecules at specific adsorption sites on graphite.[61] Our theoretical simulations with the consistent valence force field (CVFF) and the experimental high resolution STM images displayed that the CuPc and copper-hexadecafluoro-phthalocyanine (F_{16}CuPc) molecules with a four-fold symmetry favor to lie flat on HOPG.[28,62] The π-π interactions between the CuPc (F_{16}CuPc) molecules and the upmost graphite layer of HOPG are maximized in the lying down configurations with the ordered π-π stacking array parallel to surface. Interestingly, the replacement of graphite layer with the

octane-1-thiol SAM terminated Au(111), called C8-SAM/Au(111) substrate made the CuPc (F_{16}CuPc) molecules standing upright on the C8-SAM modified Au(111)surface.[39] It is hence a very useful way to manipulate the interfacial electronic structures and functions of organic films by controlling the molecular orientation with different substrates, in particular for their applications in organic field transistors and organic photovoltaics. From our multi-scale simulation combing the MD simulations with density functional theory (DFT) calculations, the carrier mobility of the standing-up CuPc (F_{16}CuPc) film was predicted to be about 10~1000 fold versus the lying-down orientations on different substrates.[62] *In-situ* synchrotron-based photoemission spectroscopy also revealed that the charge transfer at the standing F_{16}CuPc/CuPc or CuPc/F_{16}CuPc interface is much larger than that at the lying F_{16}CuPc/CuPc or CuPc/F_{16}CuPc interface.[39]

To fabricate high-performance organic thin-film transistors, many functional materials such as Pn and its functionalized derivatives were deposited on the SiO_2 substrate. The interfacial interactions between Pn and SiO_2 substrate were investigated by using the sophisticated QM calculations at the MP2 (second-order Møller-Plesset perturbation theory) level and the MM method with the CVFF, indicating that the adsorption of Pn on SiO_2 substrate is dominated by the vdW interaction.[24] For those surface mounted SAMs with the non-specific and isotropic interfacial interactions, the control of intermolecular interactions is crucial to determine the growth dynamics, packing structures, and functions of the ultra-thin films.

Site-specific interfacial interactions with metal surfaces. Different from the graphite and SiO_2 substrates, some metal surfaces take an advantage of forcing the building units to assemble into well-ordered structures through the strong molecule-substrate interfacial interactions. The DFT optimizations indicated that π-conjugated (such as Pn and PTCDA) molecules adopt the lying-down configuration with their conjugated π-plane parallel to Ag(111) and the phenyl rings lying above the Ag atoms (Fig. 3b).[26,29,35] Such an adsorption structure may allow the effective coupling between the π-electrons in molecules and the metal *d*-orbitals of metal surfaces. The most favourable geometry with the π-conjugated six-membered ring facing the topmost metal atom is also applicable to rationalize the structure of the other adsorbed molecules on Ag(111) and Au(111) surfaces. For example, when the C_{60} molecules are deposited on Ag(111) surface our MD simulations with the polymer consistent force field (PCFF) demonstrated that the hexagon and 6:6 bond orientations of the C_{60} molecule appear in abundance with the percentages of 26.3% and 37.5%, respectively, in good agreement with the experiments (hexagon: 32.2%; 6:6 bond: 38.4%).[35] The hexagon (or 6:6 bond) orientation represents a hexagon (or an inter-ring bond between two neighbouring hexagons) is facing the metal substrate, for which the coupling between the π-electrons in hexagon and the metal *d*-orbitals is maximized. The metal substrate, therefore, could act as a checkerboard to restrict the lateral degrees of freedom of the adsorbed functional molecules.

Extensive validations of CVFF or PCFF have been done by comparing the force field potential curves with MP2 and DFT calculation results, implying that the interfacial interactions were described well by the classical force fields in most cases. For the thiols modified Au (111) surface, however, the Au…S complexation interaction is stronger than the vdW interactions. In other words, the vdW term (Eq. (1)) failed to give accurate results of the interaction energy between the thiol-containing SAM and the Au(111) surface.

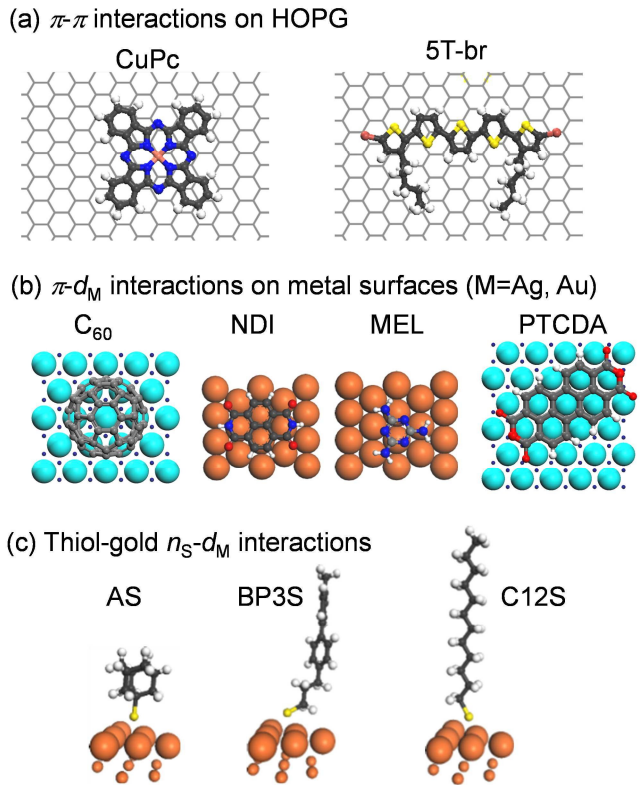

Fig. 3 Three types of interfacial interactions, (a) π-π interaction between CuPc/5T and HOPG surface, (b) π-d_M interaction between C_{60}/NDI/MEL/PTCDA and Ag(111)/Au(111) surface, and (c) n_S-d_M interaction between thiols (adamantane thiol (ASH), ω-(4′-methylbiphenyl-4-yl)propane thiol (BP3SH), and dodecane thiol (C12SH)) and Au(111) surface.

$$V_{vdw} = 4\varepsilon\left[\left(\frac{\sigma}{r}\right)^{12} - \left(\frac{\sigma}{r}\right)^{6}\right] \quad (1)$$

where ε is the well depth, σ is the distance at which the intermolecular potential is zero, r is the distance between two particles.

To solve this problem, a Morse potential (Eq. (2)) was introduced to simulate the Au-S interaction.

$$V_{Morse} = D\left[1 - e^{-\alpha(r-r_0)}\right]^2 \quad (2)$$

where D and α are the force constants and r_0 is the equilibrium bond length. The modified Morse potential can reproduce the energy profiles by MP2 calculations.[29] Such a Morse type Au-S potential was applied to elucidate the mutual influence of the deposited thiols on the intermolecular and interfacial interactions. As shown in Fig. 3c, three kinds of thiol molecules were selected in terms of different flexibility and aromatic properties.

3.2 Monolayer morphology controlled by intermolecular interactions

The morphology of monolayer is determined by the competition between the intermolecular and interfacial interactions on the surface. When the substrate-molecule interfacial interactions are similar for each building block, the intermolecular interactions play an essential role in the modulation of packing structures. Particular interest was aroused for the monolayers of *n*T and Pn derivates which are applicable in organic photovoltaic cells, organic field-effect transistors.

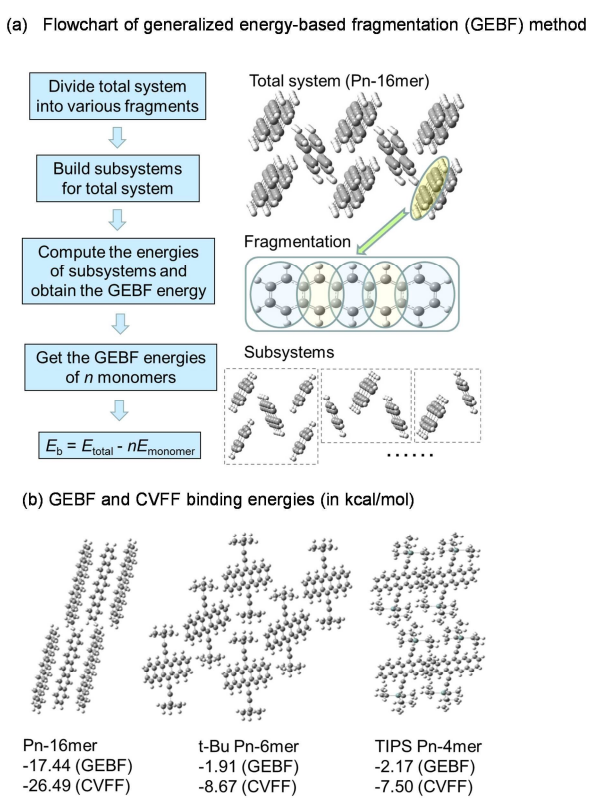

Fig. 4 Evaluation of binding energies of packing systems with (a) the generalized energy-based fragmentation (GEBF) method and (b) The GEBF and CVFF binding energies (in kcal/mol) for Pn-16mer, t-Bu Pn-6mer, and TIPS Pn-4mer, respectively.

Dominant vdW interactions between the non-polar units. It has been reported that DFT method lacks the long-range attractive component in the non-bonded interaction,[63,64] which plays an important role in binding interactions in oligomers. Some new DFT functionals such as M06-2X, CAM-B3LYP, and wB97X-D were developed to improve the performance of DFT calculations for the systems with noncovalent interactions. In order to predict the interaction energies more accurately, high-level electron correlation methods such as MP2 or coupled cluster (CC) methods are required. However, conventional MP2 or CC methods are very expensive for the large-sized systems due to their high computational scaling of N_b^{α} (where N_b is the number of basis sets and $\alpha \geq 5$). The generalized energy-based fragmentation (GEBF)[65–71]approach is an effective way for a MP2 or CC calculation with a linear scaling ($\alpha \approx 1$).

In Fig. 4a, we take the aggregate of 16 pentacene molecules (Pn-16 mer) as an example to illustrate the basic steps for computing the GEBF binding energies. In the first step, we divide each pentacene unit into five benzene-like fragments as displayed in Fig. 4a. Thus, there are 80 fragments in total. From those fragments, we build a series of GEBF subsystems, some of which are shown in Fig. 4a. Then we compute the energies of all the subsystems and obtain the GEBF energy by a linear combination.[67] It should be noted that the overlap atoms between two neighbouring fragments within each pentacene unit will be automatically cancelled according to the rule of construction of subsystems with the frame of GEBF. Furthermore, we could get the GEBF energies of monomers a similar way. Finally, the GEBF binding energy could be obtained from the GEBF total energy and GEBF energies of monomers. The calculated value for Pn-16mer is -20.54 kcal/mol.[24]

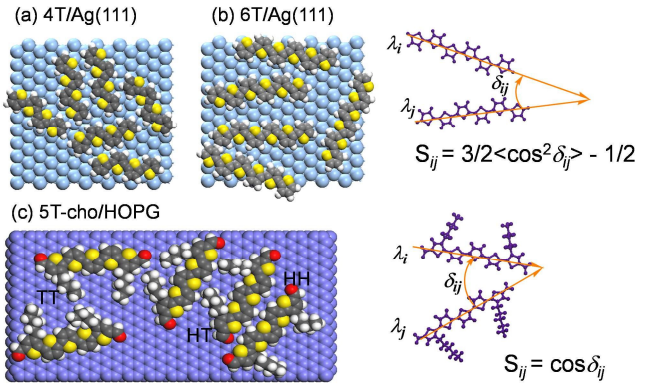

Fig. 5 Representative packing structures of oligothiophenes and the definition of the order parameter, S_{ij}, as exemplified by the snapshots of 4T (a) and 6T (b) monolayers on Ag(111) surfaces, and (c) 5T-cho on HOPG.

To investigate the relative contribution of electrostatic energy (E_{ele}) versus vdW interaction (E_{vdw}), the absolute value of ratio between the electrostatic and van der Waals interactions is defined as E_{ele}/E_{vdw}. In the packing system of 10 Pn molecules, the vdW interaction is dominate in the intermolecular interactions with the ratio of E_{ele}/E_{vdw} being 0.04 (Fig. 4b). The introduction of t-Bu and TIPS substituents in pentacene leads to the increase in electrostatic interaction (t-Bu Pn-6mer: E_{ele}/E_{vdw}=0.43; TIPS Pn-4mer: E_{ele}/E_{vdw}=0.59) relative to the unsubstituted Pn. The difference in the intermolecular interactions leads to the different packing structures and growth process of the substituted pentacenes from those of Pn. As the substituent group increases, the functionalized Pn monolayers become more orderly.[24]

Electrostatic interaction between the polar units. As discussed above, the substituent group has significant effect on tuning the relative contribution of electrostatic energy to the vdW interaction in the intermolecular interactions. Here the oligothiophenes *n*T (with *n*=4, 5, 6) are selected to show the different roles of vdW and electrostatic interactions played in manipulation of the packing morphology.

The order of the packing structures of sexithiophene (6T) and quaterthiophene (4T) was compared in both their monolayers and bilayers on the surfaces by the order parameter, which was defined as a function of the crossing angle, δ_{ij}, shown in Fig. 5. From the increasing of the order parameter against the coverage, we could see the 6T monolayer became more ordered faster than 4T monolayer, which is due to the stronger intermolecular interaction in 6T than that in 4T.[30,35] Different from 4T and 6T,the morphology of the monolayer of the disubstituted 3,3-dipentyl-α-quinquethiophenes (5Ts) with polar substitution groups of formyl (5T-cho) or bromine (5T-br) deposited on HOPG surface is largely determined by the electrostatic interaction.

There are three possible arrangements in 5T dimers, which are noted as head-to-head (*HH*), head-to-tail (*HT*), and tail-to-tail (*TT*) in Fig. 6 and Tables S1-S2. Binding energies between 5T dimers along two directions, i.e., parallel with and perpendicular to the long axis of 5T chain, are investigated by QM calculations in each arrangement and listed in Fig. 6. As mentioned in section 2 that the substituted 5Ts are polar units with the nonzero dipole moments (5T-cho: 6.9 Debye; 5T-br: 2.7 Debye). Thus, the head-to-head packing style is stabilized by the favourable dipole-dipole interactions with the opposite directions of the dipole moments of two units. The larger magnitude of dipole moment of 5T-cho than 5T-br implies the stronger binding interactions among the 5T-cho

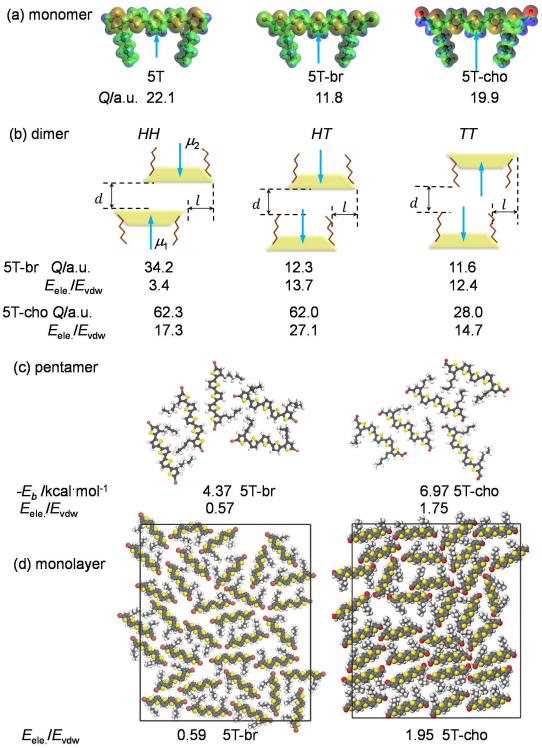

Fig. 6 GEBF-MP2 binding energies, $-E_b$ (in the unit of kcal/mol), the ratio between the electrostatic and van der Waals interactions, E_{ele}/E_{vdw}, quadrupole moments, Q (in the unit of a.u.) in 5T monomers (a), dimers (b), pentamers (c), and monolayers (d).

aggregate than the bromine-substituted one, which is supported by the GEBF-MP2 binding energies of the pentamer aggregates (5T-cho: 6.97 Kcal/mol; 5T-br: 4.37 Kcal/mol). The electrostatic interaction may become the main driving force of assembling the polar substituted oligothiophene molecules into a SAM. As expected, the absolute values of the ratio of E_{ele}/E_{vdw} of the packing systems with the two and five monomers, respectively, are much larger than 1, indicating the dominant contribution from the electrostatic interactions between the polar units.

The electrostatic interactions can be conveniently described in terms of dipole-dipole interaction, which is defined as follows,

$$E_{\mu_i\mu_j} = \sum_{i<j}^{N} k_{ij} \frac{|\mu_i|\cdot|\mu_j|}{|r_{ij}|^3}(\cos\delta - 3\cos\tau\cdot\cos\omega) \quad (3)$$

where μ_i and μ_j are the dipole moments of the ith and jth 5Ts, respectively. K_{ij} is the force constant. The centre distance of 5T dimer is r_{ij}. The angles between three vectors μ_i, μ_i, and r_{ij} are δ, τ, and ω, as shown in Fig. S1. The dipole-dipole interaction, $E_{\mu\mu}$, is calculated in both 5T dimers and monolayers at their optimal structures in Table S3. A negative value of $E_{\mu\mu}$ means the dipole-dipole interaction is attractive, and a positive value indicates the dipole-dipole interaction is repulsive. From Table S3, it is also found the dipole-dipole interaction is stronger in the 5T-cho monolayer than in the 5T-br monolayer, which originates from the stronger polarity of the 5T-cho than the Br-substituted unit. It should be mentioned that the electric moments are indeed of tensor properties. The quadrupole is written as a 3×3 matrix with 9 components (a rank 2 tensor). Besides the dipole-dipole interaction, the higher quadrupole-quadrupole interaction may also give some contribution to the electrostatic interactions. The quadrupole moments in 5T monomers and dimers are calculated by DFT method as shown in Table S4. The complicate expression of the quadrupole with the multicomponent terms makes it difficult to directly compare the relative strength of the quadrupoles between different molecular systems. The value of Q, as defined in Eq. (4), is then used to simplify the tensor expression of quadrupole moment.

$$Q = \sqrt{\frac{2}{3}(Q_{xx}^{\ 2} + Q_{yy}^{\ 2} + Q_{zz}^{\ 2})} \quad (4)$$

The quadrupole moment is reduced by the inclusion of substituents in 5T monomers, and it is stronger in 5T-cho dimer than in 5T-br dimer. The interactions between the two dipoles and quadrupoles decay with the separation r as the functions of r^{-3} and r^{-5}, respectively.

Computational results of both the dipole-dipole interaction and the relative strength of quadrupoles for 5Ts aggregates uniformly show the electrostatic interaction is stronger in 5T-cho than in 5T-br monolayer. The electrostatic interaction is almost twice of the van der Waals interaction in the 5T-cho monolayer (E_{ele}/E_{vdw} =1.95), while in the 5T-br monolayer it is just around half of the van der Waals interaction (E_{ele}/E_{vdw} =0.59). Such significant electrostatic interactions in 5T-cho monolayer render a more ordered packing structure than the 5T-br monolayer, as demonstrated by the order parameters, S_{ij} (whose definition is shown in Figure 5c).

If all the units packed in a parallel and ordered array, the order parameter is close to 1. The larger value of $|S|$ (of 0.84) in 5T-cho monolayer than that (0.73) of the 5T-br packing system does show the more ordered packing morphology of 5T-cho monolayer than the Br-substituted counterpart (Table S3). To compare with the value of $|S|$ of 4T and 6T monolayers, the monolayer of 5T with the side substituted chains are less ordered than that of 4T and 6T without side chains.

The electrostatic interaction between the polar units not only plays an essential role in determining the packing conformation, but also brings a chance to give a response to the stimuli of external electric field. Then it will be quite promising to design functional molecular wires with the tunable packing structures and properties with the application of polar units and electric filed. The simulations of such polarizable systems under the electric field urgently call for the development of efficient polarizable force fields. Conventional force field does not treat well of the electrostatic interaction, since the partial charge of each atom is fixed all the time during the MD simulations of conformational changes. However, the charge should be changeable, which is induced by the dipole-dipole interaction between the polar units under the electric field. Thus the polarizable force field is needed to improve the calculation of electrostatic interactions by a better scheme of charge calculation. The QM-based polarizable force field has been used successfully in the description of the conformational changes in monolayers on switchable surfaces with the application of electric field.[18,19]

Complex assembly formed by cooperative hydrogen bonding interactions. Hydrogen bonding (HB), a kind of directional intermolecular interaction is widely used as a driving force for fabricating the packing pattern of binary molecular system on the surface. The formation of the complex HB network could guide the molecules to assemble into many beautiful patterns, such as honeycomb networks, chessboard, and even chiral supramolecular structures (Fig. 7).

However, hydrogen bonding only plays a part in a short-range, which could lead to an ordered dimer or trimer molecular structures. The long-range ordered molecular arrangement requires a strong interfacial interaction or substrate-mediated long-range intermolecular interactions. By means of multiple intermolecular H-bonding and interfacial interaction, a 2-D Pn:PTCDA chiral network

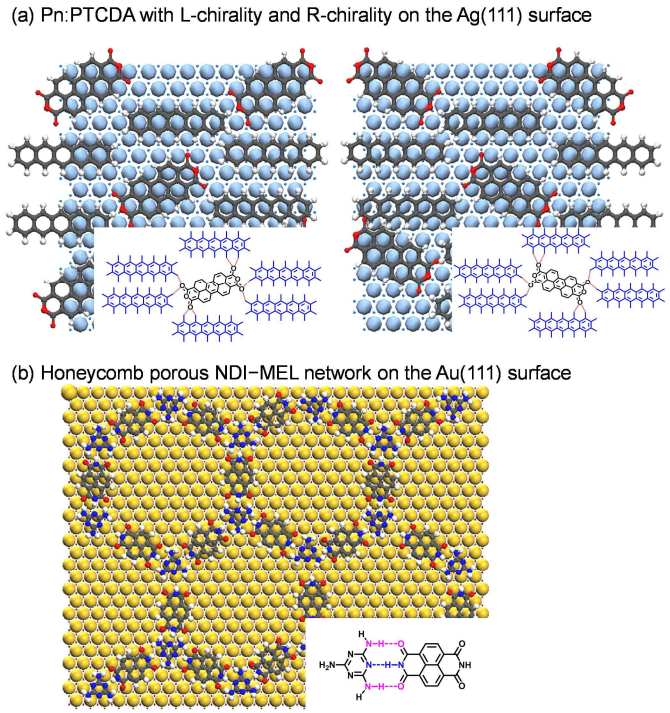

Fig. 7 Self-assembly of the binary molecular (a) NDI-MEL network on the Au(111) surface and (b) Pn:PTCDA on the Ag(111) surface with the H-bonding shown in the insets.

had been observed by STM on the Ag(111) surface.[26] The molecular structure is stabilized by the H-bonding, which is presented in Fig. 7a. A honeycomb porous NDI-MEL hybrid structure was predicted to deposit on the Au(111) surface (Fig. 7b). To simulate these supramolecular structures, a good description of both interfacial and multiple H-bonding is fundamental in DFT and MD simulations. A large slab model will be needed to include the binary molecular system in the DFT calculation, which will not be feasible in a real-time simulation. So we have used the MM calculation for such hybrid structure. The parameters in terms of vdW forces have been modified in the intermolecular and interfacial interactions, according to the binding energies in QM calculations. As a result, these hybrid networks have been well produced by dynamics simulations in our previous work.[26,29]

SAM with potential organic ferroelectric properties. Ferroelectricity, a property that enables switching electric polarization under the influence of an external electric field, has been widely applied in random access memories, dynamic random access memory capacitors, field-effect transistors, electron emitters, and weak-magnetic field sensors for inorganic ferroelectric materials.[72,73] However for light, flexible, and nontoxic organic ferroelectrics, only polyvinylidene fluoride (PVDF), whose repeating unit owns a permanent dipole moment, and its related copolymers have been used to fabricate real devices, such as ferroelectric field-effect transistors[74,75] and solar cells[76] until now. In organic ferroelectrics, polarization comes from dipoles in a non-centrosymmetric lattice. As shown in Fig. 8a, CA and 3-HPLN molecules with intrinsic dipoles (5~6 Debye in Fig. 2) form single-component molecular crystals through supramolecular interactions, including dipole-dipole interaction, hydrogen bonding, or π–π stacking. These CA and 3-HPLN crystals have the room-temperature ferroelectricity with the maximal spontaneous polarization along the crystallographic c and a axes, respectively. The polarization in these crystals is switched by the chemical-structure change

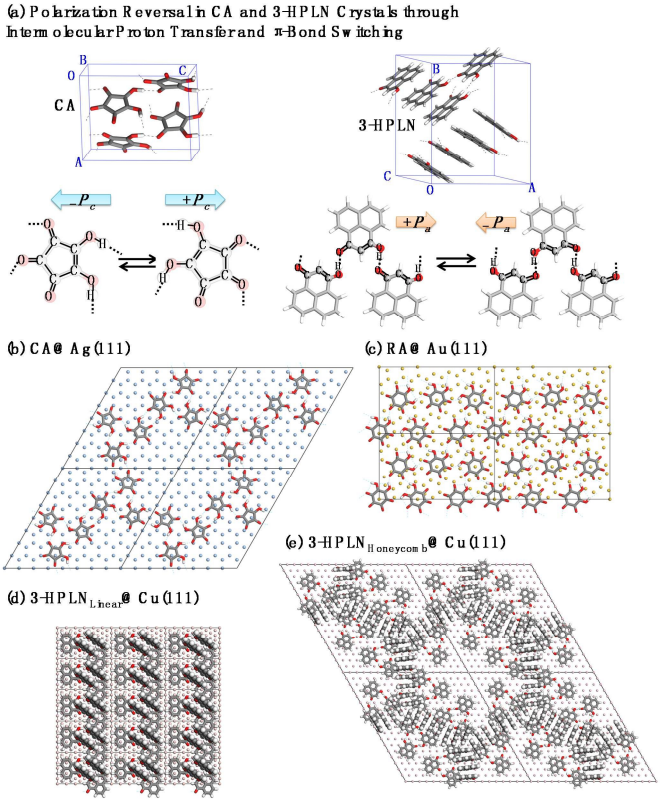

Fig.8 (a) Schematic illustration of polarization reversal in CA and 3-HPLN crystals through intermolecular proton transfer and π-bond switching and 2-D self-assembly of organic ferroelectrics: (b) CA monolayer on Ag(111) surface, (c) RA monolayer on Au(111) surface, (d) 3-HPLN linear-like bilayer on Cu(111) surface, and (e) 3-HPLN honeycomb-like bilayer on Cu(111) surface.

resulting from intermolecular proton transfer and π-bond switching (Fig. 8a). With reference to their ferroelectric crystals, the CA and 3-HPLN molecules can be used as self-assembled units to form 2-D orderly networks on metal substrates through supramolecular interactions between molecules and molecule-substrate interaction[40,77] to fabricate ferroelectric films for potential device application. Similar to CA molecule, RA molecule is still a member of a series of planar monocyclic oxocarbon acids, $H_2C_nO_n$, where n = 3~6, and its molecular dipole (about 5 Debye) are within the molecular planes in Fig. 2. Although RA is hygroscopic and its crystal exhibits in the form of RA dehydrate,[78] the RA molecules could be deposited on Au(111) surface to form 2-D self-assembled monolayer under ultrahigh vacuum at room temperature in Fig. 8c.[40] For these self-assembled monolayers or bilayers on metal surfaces, the complex interactions on surface would further result in induced dipoles, for example of charge transfer between molecules and substrate. Just because of these subtle interactions on metal surfaces, these SAMs or bilayers would be symmetry-breaking to finally own net polarization. Although the polarization state of the 2-D networks is not experimentally feasible with current techniques, theoretical simulations can be used to predict the polarization switching of ferroelectric monolayers on metal surfaces under an applied electric field.[41]

For the CA monolayer on Ag(111) surface in Fig. 8b, the hydrogen-bonded CA dimers can be treated as the elementary building block to form triangular-shaped clusters.[77] For the RA monolayer on Au(111) in Fig. 8c, RA molecules forms extended hydrogen-bonded network exhibiting hexagonal symmetry.[79] The

proton transfer occurs spontaneously within the CA monolayer at room temperature. In contrast, no proton transfer is observed in RA monolayer at room temperature, even under a relatively large electric field.[41] For both CA monolayer on Ag(111) surface and RA monolayer on Au(111) surface, thermal structural fluctuations at room temperature would induce large variations of in-plane polarization, and even further mask electric-field-induced polarization switching.[41] These CA and RA hydrogen-bonded networks exhibit constant polarization normal to the metal substrates.[41] Detailed polarization estimation of CA and RA monolayers can be found in ESI subsection S1.2."

The simulations of 3-HPLN systems are more complicated than the CA and RA films. After 3-HPLN molecules are deposited on flat Cu(111) surface at room temperature, they form self-assembled bilayers consisting of two competing structures, a linear structure (Fig. 8d) and a honeycomb one (Fig. 8e),[40] whose optimization can be found in ESI subsection S1.3. In both bilayers, it appears that the molecules of the bottom layer, which maximize molecule–substrate interaction, are flat-lying on the surface, while the molecules in the top layer stand upright on the bottom layer.[40] For the linear-like bilayer (Fig. 8d), its bottom layer keeps the zigzag chains which can be found in the 3-HPLN crystal, and its top layer consists of elementary π–π stacked 3-HPLN dimers standing on zipper-like hydrogen-bonding channel. For the honeycomb-like bilayer (Fig. 8e), its top layer reserves the symmetry of a Kagome lattice. Here, the π–π stacked 3-HPLN dimer can be treated as the elementary unit to form the chiral, pinwheel-like junctions of three dimers and linear segment of two dimers connecting both junction ends. The flat-lying 3-HPLN molecules in the bottom layer, consisting of six elementary 3-HPLN hydrogen-bonded trimers, keep six-fold symmetry as the Kagome-lattice-like top layer.[40]

The above-drawn picture of tuning monolayer packing structures by both intermolecular and interfacial interactions does also work well for the assembly of biomolecules. Surface functionalization with proteins holds a lot of promise in biosensing and other biological applications. Here we just take the abundant protein, collagen, as an example. Self-assembly of collagen molecules can be aligned into a highly oriented fibrils on surfaces at controllable pH and the electrolyte concentration conditions.[80] To understand the mechanics of collagen fibrils, their assembly patterns have been revealed by the both high resolution AFM and MD simulations in various buffer solutions.[81] The assembled nanostructures are controlled by the competition between the intermolecular (collagen-collagen) and interfacial (collagen-substrate) interactions. When the interfacial interactions dominate the growth process, the collagen either assembles into a random network or orientates into a preferred direction. While in the other regime, the mobility of collagen is enhanced with the increasing of intermolecular (collagen-collagen) interactions, leading to 3-D bundles.[81] Through the theoretical study of the mechanical relationship in the collagen fibrils with a distance-dependent reactive mesoscopic model, Buehler found the natural design of collagen assembly maximizes the strength of intermolecular interactions and energy dissipation during deformation, which causing their nanopattern reproducible and tunable in various applications.[82] Collagen could be further functionalized with other proteins to build novel biosensors or biomaterials in cell biology.

4 Stimuli-responsive conformational changes of molecular monolayer on surface

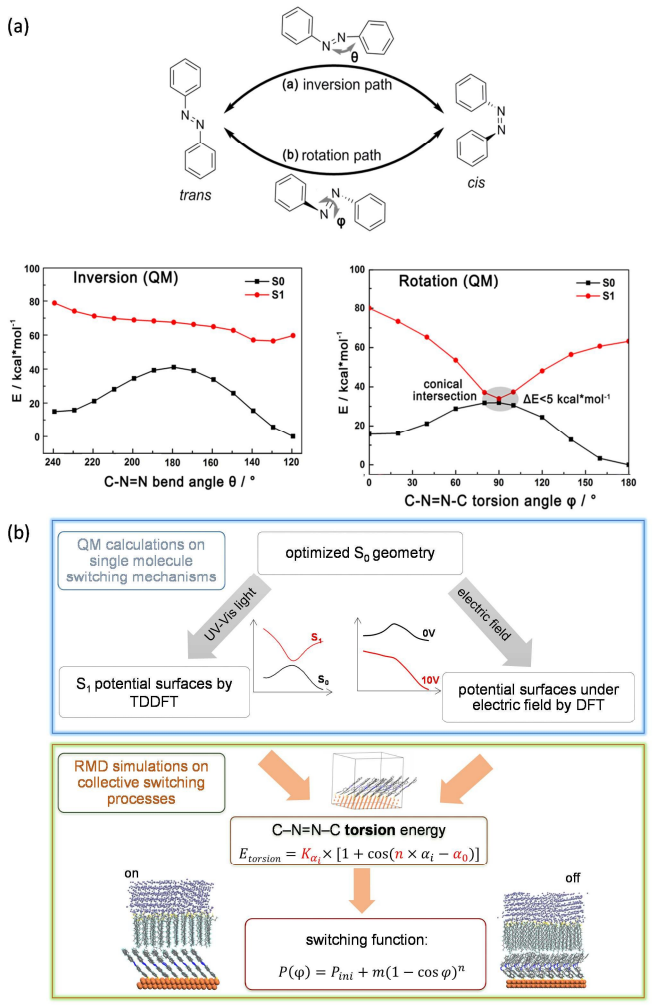

Fig. 9 (a) Isomerization of the azobenzene molecule in rotation and inversion paths. (b) The flowchart of simulations in the isomerization process of AZO monolayer on the Au(111) surface.

The introduction of the dynamic stimuli-responsive units into the surface bounded SAMs is a promising way to fabricate the smart surfaces related to the development of various nano devices. The dynamic conformational changes of surface-supported molecules determine the macroscopic morphology and property of the surface. Some molecules bear flexible backbones, so the thermal motions of atoms can trigger the conformational changes at room temperature. For examples, the rotation barrier of C-C bonds in alkyl chain and diarythene is rather low (less than 5.0Kcal/mol),[9] which is comparable to the magnitude order of KT when T is around 298 K. In this case, the MD based on the traditional force fields can be applied to simulate the conformational change of the flexible molecules on surfaces. The solvent effect on the conformational interconversion of diarythene derivatives was also revealed in an explicit solvent model by classical MD simulations.[83] It was demonstrated that the anti and twist isomers can interconvert easily, but the interconversion between anti and para isomers is more difficult due to a higher energy barrier.

However, the photo induced cis/trans transformations of AZO derivatives are achieved by UV light, in order to overcome the much higher rotation barrier (of about 20 kcal/mol) of N=N bond. Note that the process of photo-triggered conformational interconversion is not in the equilibrium. The non-equilibrium MD simulations were

thus introduced to analyse the dynamics of the photo-switchable process of AZO-based aggregates in solutions or monolayers on surfaces.[36–38,44,45] Traditional force fields with harmonic potentials are good at describing the equilibrium geometry but not suitable for the simulations in the stimuli-driven isomerization process of AZO derivatives. Several kinds of modifications of force fields are then implemented to make some chemical bonds 'reactive'.

It has been reported that there are three possible paths for the isomerization of AZO molecule, through the torsion of the N=N bond, inversion of N=N-C bond angle, and NN-twist.[84–87] QM calculations at various theoretical levels demonstrate that the energy barrier of the inversion path is much higher than that of the torsion path in the trans/cis interconversion, as shown in Fig. 9a. The applications of reactive force fields in MD simulations of the torsion path for trans/cis interconversion have been reported for many kinds of AZO-based materials.[39,44–46]

The basic assumption underlying the reactive model lies in that the N=N rotation parameters of an isolated AZO derivative are transferable to those in complex molecular aggregates. The transferable rotational potentials of the N=N bond torsion were fitted from the QM energy profiles of a single isolated AZO molecule. The scheme of combination QM calculations and RMD are presented in Fig. 9.

The expression for 'reactive' torsion energy, E_{tor}, keeps the fundamental form of the classical force field except for the employment of different parameters of force constant and periodicity of cosine function from the traditional ones (Fig. 9b). In the simulation of trans-cis interconversion, a switching function, $P(\varphi)$, is defined as the probability of the molecule on the trans curves at torsion angle, φ.

From QM calculations of the AZOs/Au cluster model, the cis-to-trans isomerization of the polar AZO derivative could happen not only by the stimulation of radiation, but also by the stimulation of the electric field.[36] It is interesting to notice that the trans-to-cis interconversion of AZO only happens in the photoisomerization process. The driven force of the isomerization processes induced by the electric field is complicated by involving with the charge transfer at the interface.[36] It was also demonstrated by our MD simulations that the collective cis-to-trans switching behaviour of the hundreds of the polar AZO derivatives enables the AZO-based SAM to lift the alky thiol coated mercury droplet with an Au(111)-SAM_{AZO}//SAM_{C12}-Hg molecular junction model under the light radiation or electric field.[36] This junction model can be taken as a prototype of a smart cargo lift under the electric field.

5. Entropy changes in formation process of SAMs

Theoretical simulations have provided insight to manipulate the formation of SAMs with the subtle interplay between intermolecular interactions of building units and the substrate-molecule interfacial interactions. However, the formation process of a SAM is also controlled by the kinetics of molecular aggregation and nucleation. It is still difficult to directly detect the formation process of the molecular cluster or the first layer on surface in experiment. To this end, theoretical simulations can provide the detailed packing structures of ultra-thin films and even the dynamic processes of film growth. Due to the complexity in the theoretical model of the surface-supported SAM, few simulations have been carried out to estimate the entropy changes during the film growth. Recently, we proposed a model to estimate the changes in the pack entropy, S_{pack}, and free energy, F, during the formation of SAM from

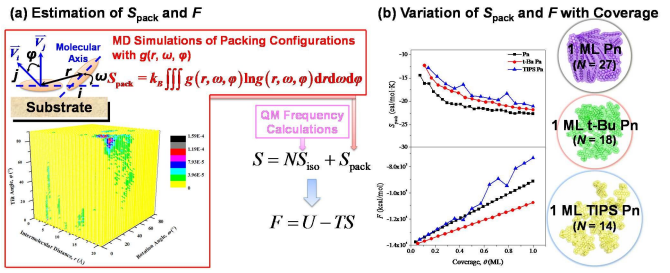

Fig. 10 (a) Graphical presentation of estimation of packing entropy, S_{pack}, and free energy, F. The packing entropy, S_{pack}, is estimated based on pair distribution function, g(r, ω, φ), which is obtained from MD simulations of packing configurations characterized by three degrees of freedom, r, ω, and φ, between two deposited molecules, i and j, in functionalized Pn aggregates. (b) variation of S_{pack} and F with the coverage, ϑ, during the initial nucleation of Pn, t-Bu Pn, and TIPS Pn molecules on SiO_2 surface. The 400-ps snapshots of 1-monolayer (ML) functionalized Pn are highlighted in insets.

a series of MD snapshots obtained by adding molecules on by one, with the flowchart and results shown in Fig. 10.[24]

On the molecular scale, the entropy can be expressed as a series of the n-particle correlation functions.[88–90] With the two-particle approximation, the entropy contribution of the molecule aggregate with the cluster size, N, can be grouped into two parts, isolated and packing ones,

$$S = NS_{iso} + S_{pack} \quad (5)$$

where S_{pack} only considers the interactions between two packing molecules taken from N deposited functionalized Pn molecules.

The entropy of a single isolated molecule can be approximately evaluated from the QM frequency calculations, consisting of the contribution from the degrees of translation, S_{iso_trans}, rotation, S_{iso_rot}, and vibration, S_{iso_vib}, freedom. An emphasis is then laid on the packing entropies of molecular aggregates. Since entropy is an expression of disorder or randomness in the statistical mechanism, the packing entropy can be further estimated from the degree of order of aggregates. As addressed in Section 3, the order parameter of the stacked array is often adopted to reflect the degree of order of these monolayers. Then, the key lies in the statistical analysis of the packing structures.

For the nearly-planar π-conjugated molecule, a certain packing configuration for two deposited molecules, i and j, can be described by the intermolecular distance, r (the distance between centres of mass of two molecules), rotation angle, ω (the angle between the molecular axes of two Pn cores), and tilt angle, φ (the angle between the normal vectors, $\vec{V_i}$ and $\vec{V_j}$ of two Pn cores), as shown in Fig. 10a. Then, a pair distribution function, g(r, ω, φ), is defined in terms of both the radial (r) and orientational (ω, φ) correlation of the packing pairs,

$$g(r,\omega,\varphi)dr d\omega d\varphi = \frac{N_{pair}(r,\omega,\varphi)}{N_{pair}} \quad (6)$$

where $N_{pair}(r, \omega, \varphi)$ is the number of packing pairs with a specific intermolecular distance, r, rotation angle, ω, and tilt angle, φ, and N_{pair} is the total number of the packing pairs in films. Individually, the radial distribution function, $g(r)$, and orientational distribution functions, $g(\omega)$ and $g(\varphi)$, can be defined in a similar way.

The pair distribution function, $g(r, \omega, \varphi)$, can be obtained from the statistical results of the MD simulations. Then, the Boltzmann formula (where k_B is the Boltzmann factor) is used to estimate the

packing entropy according to the radial and orientational freedom of packing configurations, i.e.,

$$S_{pack} = k_B \iiint g(r,\omega,\varphi) \ln g(r,\omega,\varphi)\, dr d\omega d\varphi \quad (7)$$

The implementation of this packing entropy model was inspired by the successful application of the orientation function to calculate the orientational entropy in liquid crystals.[91,92]

Taking the Pn and its functionalized derivatives as an example, different substituent groups cause different packing behaviours during the film growth on the amorphous SiO_2 surface. During the nucleation, the rod-like Pn molecules tend to diffuse rapidly and have different orientations on the SiO_2 surface. Upon the molecular aggregation of Pn and its derivatives, the packing entropy, S_{pack}, first decreases dramatically and then gradually converges to a constant as the coverage increases in Fig. 10b. As the size of substituents increases from Pn, t-Bu Pn, to TIPS Pn, the functionalized Pn aggregates become more orderly with the increasing degree of order. When the cluster size of molecular aggregates is larger than critical nucleus size, adding more molecules (even with quite different orientations) does not change the degree of order of films much. The contribution of packing entropy to the free energy is slightly positive, which means a small entropic barrier (less than 7.5 kcal/mol at room temperature) should be overcome for the aggregation of functionalized Pn molecules on the SiO_2 surface. As shown in Fig. 10b, the free energies of Pn and t-Bu Pn increase linearly with the coverage, and in the initial nucleation, the free energy of t-Bu Pn is a little smaller than that of Pn at the same coverage.

It is hence useful to correlate our simulation results[24] with experimental observations.[93–99] Our simulations exhibit that the rod-like Pn molecules lie down with various orientations, and tend to stand up as the coverage increases.[24] In the orderly bulk phase of Pn thin films, most of the Pn molecules would stand upright in experiments.[93–96] We also predicted that the branched t-Bu Pn and TIPS Pn molecules prefer to lie parallel to the substrate in the low coverage.[24] Occasionally, the TIPS Pn molecule would stand up in our simulations.[24] This is in agreement with kinetically trapped TIPS Pn molecules undergo "reorganization" to finally form the orderly thin film in which TIPS Pn molecules align with the acene unit "edge-on" oriented touching down with the TIPS groups.[97–99] This occasional change of TIPS Pn from lying-down orientation to standing-up would induce "jump" in the calculated free energy landscape[24] (Fig. 10b). Our free energy picture has also been used to understand formation of kinetically trapped nanoscale grains with different molecular orientations in solution-cast TIPS Pn thin films.[100] Details for estimation of entropy and free energy can be found in ESI Subsection S1.4.

6. Summary and perspective

Through a small number of paradigmatic examples, the cooperation between the theoretical simulations and experimental investigations has been demonstrated to be of a significant connection between the microscopic electronic structures and the macroscopic optical, electric, and mechanical properties of some functional organic materials in biology and nanotechnology. The recent achievements in this direction, some of which have been recalled here, seem to indicate that the understanding of the nature of interactions between the building units and interfacial interactions will guide the rational design of various functionalized SAMs on surfaces with the desired packing morphology and function. The linear scaling QM calculations and the modified force fields have been applied to study the interaction energies between the function units. The experimental images related to the packing morphology were successfully rationalized by QM and MM simulations. The functions and the formation processes of SAMs were also investigated by the newly developed multi scale methods and the packing entropy model, respectively. Reactive force fields along with the switching function were employed to simulate the dynamic switching processes of stimuli-responsive SAMs on surfaces.

Although much progress has been made in theoretical models, many significant opportunities remain for extending the applicable scope of the existent methods to the realistic scale of the SAM deposited on various surfaces. One urgent target is to develop the linear scaling QM method to treat the large-scale cooperative intermolecular interactions in SAMs with 2-D periodicity. Recently, the fragment-based linear scaling QM methods have been implemented to predict the lattice energies and structures of molecular crystals with three-dimensional periodicity.[101–107] Within those approaches, the GEBF approach under PBC can be employed for various systems at high electron correlation levels by taking the long-range electrostatic interaction of the infinite crystal environment into account.[107] Future efforts are required to apply the fragment-based QM models to estimate the thermodynamic stability of SAM with the presence of the vacuum layer on top of a slab model. With this, the most favourable 2-D packing structure can be predicted before the experimental fabrication.

A second area of methodology developments is the simulation of the dynamic behaviours of SAMs in both quasi-equilibrium states (formed from non-polar or polar units) and out-of-equilibrium switching process (for the stimuli-responsive units). The evaluation of change in entropy is crucial to understand the driving force and dynamics of the formation of molecular aggregates and phase transition. The quantitative determination of entropy is rather difficult both experimentally and theoretically. Some theoretical models were applied to calculate the entropy contributions on the basis of the statistical results of Monte Carlo (MC) or MD simulations on several kinds of systems. Our computational method for packing entropy estimation can be extended to arbitrary molecules with rigid backbones like π-conjugated organic molecules to understand the driving force of self-assembly and aggregative behaviours of these molecules, whose degrees of freedom can be described by radial and orientational parameters during nucleation. For other flexible molecules, our two-particle approximation for estimation of packing entropy combined with careful choice of characteristic parameters to represent degrees of freedom of these molecules would still work. With the introduction of the dynamic switching unit, however, the description of changes in entropy and free energy during the switching process is a big challenge. The structure of the deposited monolayer is reorganized in fabrication of the switchable surface under external stimuli. The presence of an external electric field also leads to a redistribution of atomic charges in the monolayer. In this situation, the traditional MD simulation the fixed partial charges in the electrostatic interactions fails in the description of smart surfaces stems. The new developments and challenges in building polarizable force fields have been highlighted in recent publications.[108,109] In terms of external stimuli, there are various types of them, such as optical, electric/magnetic field, thermal, and chemical/biochemical stimuli. These stimuli convert solar or chemical/bio energy into electronic energy by the controllable monolayers, but the energy conversion efficiency in these devices is still too low to be used in any real-word technology.

Finally, SAMs provide a platform to generate macroscopic optical and electric properties and functions from the molecular-scale design, synthesis, and assembly. The use of multi-scale or multi-level methods with the combination of different hierarchical levels of theoretical models can bridge the gap between the electronic structures of building units and the macroscopically observable phenomena (such as the conductivity and emission spectra).[62,110,111] Various multi-scale strategies were proposed to connect the quantum to the mesoscopic level by using the QM, classical force fields, and coarse grained simulation models.[112] Especially for the applications of SAMs in molecular electronics, some unprecedented insights have been gained into how the electronic and optical properties are affected by factors of the structure, orientation, and interface between SAMs and their electric contacts.[113–115] However, few works were devoted to the design of novel materials with ferroelectricity, piezoelectricity, and some other intriguing properties.[116,117] Probing the polarization properties of the 2-D networks is experimentally not feasible with current techniques. It is hence necessary and challenging to develop computational technologies and methods to first obtain different polarization states of 2-D self-assembled structures at atomic scale and then to accurately calculate their polarization values.[41] Theoretical calculations can be also applied to design the multi-component 2-D self-assembled structures based on diverse organic ferroelectrics.

In addition, molecular quantum-dot cellular automata (MQCA) is a novel alternative approach for building the next-generation microelectronic elements.[118] In MQCA, binary information, 0 or 1, is encoded in the bistable charge configuration of a cell system. The Coulomb interaction between neighbouring cells provides device-device coupling for information transfer with no current flow and low power dissipation.[119] To realize controllable fabrication and operation of MQCA, the molecules need to be attached to a substrate, such as a semiconductor or metal surface.[120] Through our MD simulations and DFT calculations, the double-cage fluorinated fullerenes, $C_{20}F_{18}(NH)_2C_{20}F_{18}$, can form ordered arrays on Ag(100) surface, which may be a promising MQCA candidate in future applications.[121] The introduction of biological units extends SAMs to the more complicated biotechnological applications such as biosensors, tissue engineering, and cell biology. There remain many opportunities to apply diverse building units to design new SAMs of major relevance to the materials, life sciences, and other exciting new applications. The development of unambiguous and predictive models is desired to establish the correlation between the structures and functions and, consequently, to "control surfaces at will", namely to spatially and temporally control their surface properties in the future.

Acknowledgements

This work was supported by the National Natural Science Foundation of China (Grant Nos. 21290192, 21273102). We are grateful to the High Performance Computing Centre of Nanjing University for doing the quantum chemical calculations in this paper on its IBM Blade cluster system.

Jin Wen received her PhD degree in Chemistry from Nanjing University under the supervision of Prof. Jing Ma in 2012. Then she has been a postdoc in the Institute of Organic Chemistry and Biochemistry, Academy of Sciences of the Czech Republic in the groups of Prof. Josef Michl and Dr. Zdeněk Havlas. Her research interests focus on the molecular dynamics simulations of self-assembly on the metal surfaces and molecular spectroscopy simulations by *ab initio* methods.

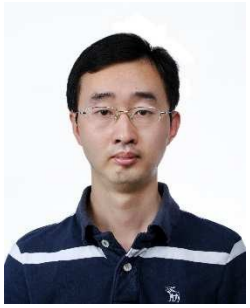

Wei Li is an associate professor at Nanjing University, China. He received his BS degree in 2002 and his PhD degree in chemistry in 2007 both from Nanjing University under the guidance of Prof. Shuhua Li. Then, he worked as a postdoc in the group of Prof. Piotr Piecuch at Michigan State University in 2007-2010. His research interests focus on the development of linear scaling algorithms for ab initio calculations of complex systems.

Shuang Chen is an associate professor at Nanjing University, China. She received her BS degree in chemistry from Nanjing University in 2005. Her PhD degree under the guidance of Professor Jing Ma was received in chemistry from Nanjing University in 2010. Later, she worked as a postdoc at Nanjing University and then University of Nebraska-Lincoln in 2012-2015. Her research interests include multi-scale simulations and ab initio molecular dynamics simulations of nanomaterials, especially for self-assembled structures on surfaces and film growth mechanism.

Jing Ma is a professor of theoretical chemistry at Nanjing University, China. She received her Ph.D. in Chemistry from Nanjing University in 1998, and after then she was awarded JSPS postdoctoral fellowship to work in Prof. Satoshi Inagaki's group in Gifu University, Japan. During 2001-2005, she was an associate professor in Nanjing University. She has received several awards, including Outstanding Young Chemist Award of Chinese Chemical Society and Chinese Young Women Scientists Awards. Her research interests focus on the development of the QM-based reactive and polarizable force fields to study conformational ensembles and properties of functional materials in condensed phase or at interfaces.

Notes and references

1 J. C. Love, L. A. Estroff, J. K. Kriebel, R. G. Nuzzo and G. M. Whitesides, *Chem. Rev.*, 2005, **105**, 1103–1170.

2 R. Madueno, M. T. Raisanen, C. Silien and M. Buck, *Nature*, 2008, **454**, 618–621.
3 A. Dmitriev, N. Lin, J. Weckesser, J. V. Barth and K. Kern, *J. Phys. Chem. B*, 2002, **106**, 6907–6912.
4 S. De Feyter, A. Miura, S. Yao, Z. Chen, F. Würthner, P. Jonkheijm, A. P. H. J. Schenning, E. W. Meijer and F. C. De Schryver, *Nano Lett.*, 2005, **5**, 77–81.
5 S. D. Feyter and F. C. D. Schryver, *Chem. Soc. Rev.*, 2003, **32**, 139–150.
6 J. Li, C.-L. Sun, R. Shen, X.-Y. Cao, B. Zhou, D.-C. Bai and H.-L. Zhang, *J. Am. Chem. Soc.*, 2014, **136**, 11050–11056.
7 *J. Mater. Res.*, 2004, **19**, 1889–1916.
8 F. Cicoira, C. Santato and F. Rosei, in *STM and AFM Studies on (Bio)molecular Systems: Unravelling the Nanoworld*, 2008, pp. 203–267.
9 J. Lahann, S. Mitragotri, T.-N. Tran, H. Kaido, J. Sundaram, I. S. Choi, S. Hoffer, G. A. Somorjai and R. Langer, *Science*, 2003, **299**, 371–374.
10 P. M. Mendes, *Chem. Soc. Rev.*, 2013, **42**, 9207–9218.
11 I. Willner, A. Doron and E. Katz, *J. Phys. Org. Chem.*, 1998, **11**, 546–560.
12 P. Brown, C. P. Butts and J. Eastoe, *Soft Matter*, 2013, **9**, 2365–2374.
13 M. A. Cole, N. H. Voelcker, H. Thissen and H. J. Griesser, *Biomaterials*, 2009, **30**, 1827–1850.
14 K. Sato, Y. Itoh and T. Aida, *J. Am. Chem. Soc.*, 2011, **133**, 13767–13769.
15 H. Kim, J. Park, K. Noh, C. J. Gardner, S. D. Kong, J. Kim and S. Jin, *Angew. Chem. Int. Ed.*, 2011, **50**, 6771–6775.
16 C. L. Yeung, P. Iqbal, M. Allan, M. Lashkor, J. A. Preece and P. M. Mendes, *Adv. Funct. Mater.*, 2010, **20**, 2657–2663.
17 P. M. Mendes, *Chem. Soc. Rev.*, 2008, **37**, 2512–2529.
18 C. L. Yeung, X. Wang, M. Lashkor, E. Cantini, F. J. Rawson, P. Iqbal, J. A. Preece, J. Ma and P. M. Mendes, *Adv. Mater. Interfaces*, 2014, **1**, 1300085.
19 J. Zhao, X. Wang, N. Jiang, T. Yan, Z. Kan, P. M. Mendes and J. Ma, *J. Phys. Chem. C*, 2015, **119**, 22866–22881.
20 S. Chen, Y. Itoh, T. Masuda, S. Shimizu, J. Zhao, J. Ma, S. Nakamura, K. Okuro, H. Noguchi, K. Uosaki and T. Aida, *Science*, 2015, **348**, 555–559.
21 Y. Chen, E. R. Cruz-Chu, J. C. Woodard, M. R. Gartia, K. Schulten and L. Liu, *ACS Nano*, 2012, **6**, 8847–8856.
22 P. Iqbal, F. J. Rawson, W. K.-W. Ho, S.-F. Lee, K. C.-F. Leung, X. Wang, A. Beri, J. A. Preece, J. Ma and P. M. Mendes, *ACS Appl. Mater. Interfaces*, 2014, **6**, 6264–6274.
23 C. Y. Wong, B. L. Cotts, H. Wu and N. S. Ginsberg, *Nat. Commun.*, 2015, **6**, 5946.
24 S. Chen and J. Ma, *J. Chem. Phys.*, 2012, **137**, 74708.
25 Y. L. Huang, W. Chen, H. Li, J. Ma, J. Pflaum and A. T. S. Wee, *Small*, 2010, **6**, 70–75.
26 W. Chen, H. Li, H. Huang, Y. Fu, H. L. Zhang, J. Ma and A. T. S. Wee, *J. Am. Chem. Soc.*, 2008, **130**, 12285–12289.
27 K. H. L. Zhang, H. Li, H. Mao, H. Huang, J. Ma, A. T. S. Wee and W. Chen, *J. Phys. Chem. C*, 2010, **114**, 11234–11241.
28 Y. L. Huang, H. Li, J. Ma, H. Huang, W. Chen and A. T. S. Wee, *Langmuir*, 2010, **26**, 3329–3334.
29 J. Wen and J. Ma, *J. Phys. Chem. C*, 2012, **116**, 8523–8534.
30 J. Wen and J. Ma, *J. Theor. Comput. Chem.*, 2009, **8**, 677.
31 C. M. Crudden, J. H. Horton, I. I. Ebralidze, O. V. Zenkina, A. B. McLean, B. Drevniok, Z. She, H.-B. Kraatz, N. J. Mosey, T. Seki, E. C. Keske, J. D. Leake, A. Rousina-Webb and G. Wu, *Nat. Chem.*, 2014, **6**, 409–414.
32 P. C. Rusu and G. Brocks, *Phys. Rev. B*, 2006, **74**, 73414.
33 S. S. Jang, Y. H. Jang, Y.-H. Kim, W. A. Goddard, A. H. Flood, B. W. Laursen, H.-R. Tseng, J. F. Stoddart, J. O. Jeppesen, J. W. Choi, D. W. Steuerman, E. DeIonno and J. R. Heath, *J. Am. Chem. Soc.*, 2005, **127**, 1563–1575.
34 G. Heimel, L. Romaner, J.-L. Brédas and E. Zojer, *Surf. Sci.*, 2006, **600**, 4548–4562.
35 J. Wen and J. Ma, *Langmuir*, 2010, **26**, 5595–5602.
36 J. Wen, Z. Tian and J. Ma, *J. Phys. Chem. C*, 2013, **117**, 19934–19944.
37 Z. Tian, J. Wen and J. Ma, *J. Chem. Phys.*, 2013, **139**, 14706.
38 Z. Tian, J. Wen and J. Ma, *Mol. Simul.*, 2015, **41**, 28–42.
39 W. Chen, S. Chen, S. Chen, Y. L. Huang, H. Huang, D. C. Qi, X. Y. Gao, J. Ma and A. T. S. Wee, *J. Appl. Phys.*, 2009, **106**, 64910.
40 S. Beniwal, S. Chen, D. A. Kunkel, J. Hooper, S. Simpson, E. Zurek, X. C. Zeng and A. Enders, *Chem. Commun.*, 2014, **50**, 8659–8662.
41 S. Chen, A. Enders and X. C. Zeng, *Chem. Mater.*, 2015, **27**, 4839–4847.
42 Y. Zhang, G. L. Barnes, T. Yan and W. L. Hase, *Phys. Chem. Chem. Phys.*, 2010, **12**, 4435–4445.
43 T. Luo and J. R. Lloyd, *Int. J. Heat Mass Transf.*, 2010, **53**, 1–11.
44 J. Pang, Z. Tian and J. Ma, *Chem. Phys. Lett.*, 2014, **613**, 110–114.
45 Z. Liu and J. Ma, *J. Phys. Chem. A*, 2011, **115**, 10136–10145.
46 D. M. Shin and D. G. Whitten, *J. Am. Chem. Soc.*, 1988, **110**, 5206–5208.
47 M. Hasegawa, T. Ikawa, M. Tsuchimori and O. Watanabe, *J. Appl. Polym. Sci.*, 2002, **86**, 17–22.
48 Y. Okuno, S. Yokoyama and S. Mashiko, *J. Phys. Chem. B*, 2001, **105**, 2163–2169.
49 P. Krawczyk, *J. Mol. Model.*, 2009, **16**, 659–668.
50 Y. Q. Wen, J. X. Wang, J. P. Hu, L. Jiang, H. J. Gao, Y. L. Song and D. B. Zhu, *Adv. Mater.*, 2006, **18**, 1983–1987.
51 W. Feng, W. Luo and Y. Feng, *Nanoscale*, 2012, **4**, 6118–6134.
52 J. Dokić, M. Gothe, J. Wirth, M. V. Peters, J. Schwarz, S. Hecht and P. Saalfrank, *J. Phys. Chem. A*, 2009, **113**, 6763–6773.
53 Z. F. Liu, K. Hashimoto and A. Fujishima, *Nature*, 1990, **347**, 658–660.
54 B. L. Feringa and W. R. Browne, *Molecular Switches*, John Wiley & Sons, 2011.
55 L. Zhang and J. M. Cole, *ACS Appl. Mater. Interfaces*, 2014, **6**, 3742–3749.
56 V. Ferri, M. Elbing, G. Pace, M. D. Dickey, M. Zharnikov, P. Samorì, M. Mayor and M. A. Rampi, *Angew. Chem. Int. Ed.*, 2008, **47**, 3407–3409.
57 A. Ajayaghosh and E. Arunkumar, *Org. Lett.*, 2005, **7**, 3135–3138.
58 A. S. Dvornikov and P. M. Rentzepis, *Mol. Cryst. Liq. Cryst. Sci. Technol. Sect. Mol. Cryst. Liq. Cryst.*, 1994, **246**, 379–388.
59 E. Zahavy, S. Rubin and I. Willner, *J. Chem. Soc. Chem. Commun.*, 1993, 1753–1755.
60 E. Zahavy, S. Rubin and I. Willner, *Mol. Cryst. Liq. Cryst. Sci. Technol. Sect. Mol. Cryst. Liq. Cryst.*, 1994, **246**, 195–199.
61 F. Ortmann, W. G. Schmidt and F. Bechstedt, *Phys. Rev. Lett.*, 2005, **95**, 186101.
62 S. Chen and J. Ma, *Phys. Chem. Chem. Phys.*, 2010, **12**, 12177–12187.
63 A. Dreuw and M. Head-Gordon, *Chem. Rev.*, 2005, **105**, 4009–4037.
64 B. Paizs and S. Suhai, *J. Comput. Chem.*, 1998, **19**, 575–584.

65 S. Li, W. Li and T. Fang, *J. Am. Chem. Soc.*, 2005, **127**, 7215–7226.
66 N. Jiang, J. Ma and Y. Jiang, *J. Chem. Phys.*, 2006, **124**, 114112.
67 W. Li, S. Li and Y. Jiang, *J. Phys. Chem. A*, 2007, **111**, 2193–2199.
68 W. Hua, T. Fang, W. Li, J.-G. Yu and S. Li, *J. Phys. Chem. A*, 2008, **112**, 10864–10872.
69 S. Hua, W. Hua and S. Li, *J. Phys. Chem. A*, 2010, **114**, 8126–8134.
70 S. Li, W. Li and J. Ma, *Acc. Chem. Res.*, 2014, **47**, 2712–2720.
71 W. Li, C. Chen, D. Zhao and S. Li, *Int. J. Quantum Chem.*, 2015, **115**, 641–646.
72 M. Dawber, K. M. Rabe and J. F. Scott, *Rev. Mod. Phys.*, 2005, **77**, 1083–1130.
73 J. F. Scott, *Science*, 2007, **315**, 954–959.
74 R. C. G. Naber, C. Tanase, P. W. M. Blom, G. H. Gelinck, A. W. Marsman, F. J. Touwslager, S. Setayesh and D. M. de Leeuw, *Nat. Mater.*, 2005, **4**, 243–248.
75 S. J. Kang, Y. J. Park, I. Bae, K. J. Kim, H.-C. Kim, S. Bauer, E. L. Thomas and C. Park, *Adv. Funct. Mater.*, 2009, **19**, 2812–2818.
76 Y. Yuan, P. Sharma, Z. Xiao, S. Poddar, A. Gruverman, S. Ducharme and J. Huang, *Energy Environ. Sci.*, 2012, **5**, 8558–8563.
77 D. A. Kunkel, J. Hooper, S. Simpson, G. A. Rojas, S. Ducharme, T. Usher, E. Zurek and A. Enders, *Phys. Rev. B*, 2013, **87**, 41402.
78 D. Braga, G. Cojazzi, L. Maini and F. Grepioni, *New J. Chem.*, 2001, **25**, 1221–1223.
79 D. A. Kunkel, J. Hooper, S. Simpson, S. Beniwal, K. L. Morrow, D. C. Smith, K. Cousins, S. Ducharme, E. Zurek and A. Enders, *J. Phys. Chem. Lett.*, 2013, **4**, 3413–3419.
80 D. A. Cisneros, J. Friedrichs, A. Taubenberger, C. M. Franz and D. J. Muller, *Small*, 2007, **3**, 956–963.
81 B. Narayanan, G. H. Gilmer, J. Tao, J. J. De Yoreo and C. V. Ciobanu, *Langmuir*, 2014, **30**, 1343–1350.
82 M. J. Buehler, *Proc. Natl. Acad. Sci.*, 2006, **103**, 12285–12290.
83 S. Meng and J. Ma, *J. Phys. Chem. A*, 2012, **116**, 913–923.
84 L. Wang, J. Xu, H. Zhou, C. Yi and W. Xu, *J. Photochem. Photobiol. Chem.*, 2009, **205**, 104–108.
85 A. Cembran, F. Bernardi, M. Garavelli, L. Gagliardi and G. Orlandi, *J. Am. Chem. Soc.*, 2004, **126**, 3234–3243.
86 C. Ciminelli, G. Granucci and M. Persico, *Chem. - Eur. J.*, 2004, **10**, 2327–2341.
87 C. R. Crecca and A. E. Roitberg, *J. Phys. Chem. A*, 2006, **110**, 8188–8203.
88 T. Lazaridis and M. Karplus, *J. Chem. Phys.*, 1996, **105**, 4294–4316.
89 R. Esposito, F. Saija, A. Marco Saitta and P. V. Giaquinta, *Phys. Rev. E*, 2006, **73**, 40502.
90 J. Zielkiewicz, *J. Phys. Chem. B*, 2008, **112**, 7810–7815.
91 H. H. Wensink, *Phys. Rev. Lett.*, 2004, **93**, 157801.
92 M. Greschek and M. Schoen, *J. Chem. Phys.*, 2011, **135**, 204702.
93 L. F. Drummy and D. C. Martin, *Adv. Mater.*, 2005, **17**, 903–907.
94 R. Ruiz, A. Papadimitratos, A. C. Mayer and G. G. Malliaras, *Adv. Mater.*, 2005, **17**, 1795–1798.
95 H.-L. Cheng, Y.-S. Mai, W.-Y. Chou, L.-R. Chang and X.-W. Liang, *Adv. Funct. Mater.*, 2007, **17**, 3639–3649.
96 S.-W. Liu, C.-C. Lee, H.-L. Tai, J.-M. Wen, J.-H. Lee and C.-T. Chen, *ACS Appl. Mater. Interfaces*, 2010, **2**, 2282–2288.
97 J. E. Anthony, J. S. Brooks, D. L. Eaton and S. R. Parkin, *J. Am. Chem. Soc.*, 2001, **123**, 9482–9483.
98 J. Chen, D. C. Martin and J. E. Anthony, *J. Mater. Res.*, 2007, **22**, 1701–1709.
99 J. Chen, C. K. Tee, M. Shtein, D. C. Martin and J. Anthony, *Org. Electron.*, 2009, **10**, 696–703.
100 C. Y. Wong, B. L. Cotts, H. Wu and N. S. Ginsberg, *Nat. Commun.*, 2015, **6**, 5946.
101 H. M. Netzloff and M. A. Collins, *J. Chem. Phys.*, 2007, **127**, 134113.
102 S. Hirata, *J. Chem. Phys.*, 2008, **129**, 204104.
103 G. J. O. Beran and K. Nanda, *J. Phys. Chem. Lett.*, 2010, **1**, 3480–3487.
104 S. Wen, K. Nanda, Y. Huang and G. J. O. Beran, *Phys. Chem. Chem. Phys.*, 2012, **14**, 7578–7590.
105 P. J. Bygrave, N. L. Allan and F. R. Manby, *J. Chem. Phys.*, 2012, **137**, 164102.
106 J. Yang, W. Hu, D. Usvyat, D. Matthews, M. Schütz and G. K.-L. Chan, *Science*, 2014, **345**, 640–643.
107 T. Fang, W. Li, F. Gu and S. Li, *J. Chem. Theory Comput.*, 2015, **11**, 91–98.
108 X. Wang, T. Yan and J. Ma, *Int. J. Quantum Chem.*, 2015, **115**, 545–549.
109 J. Huang, P. E. M. Lopes, B. Roux and A. D. MacKerell, *J. Phys. Chem. Lett.*, 2014, **5**, 3144–3150.
110 W. Hu, J. Jiang, H. Nakashima, Y. Luo, Y. Kashimura, K.-Q. Chen, Z. Shuai, K. Furukawa, W. Lu, Y. Liu, D. Zhu and K. Torimitsu, *Phys. Rev. Lett.*, 2006, **96**, 27801.
111 L. Wang, Q. Li, Z. Shuai, L. Chen and Q. Shi, *Phys. Chem. Chem. Phys.*, 2010, **12**, 3309–3314.
112 P. Sherwood, B. R. Brooks and M. S. Sansom, *Curr. Opin. Struct. Biol.*, 2008, **18**, 630–640.
113 M. J. Buehler, A. C. T. van Duin and W. A. Goddard, *Phys. Rev. Lett.*, 2006, **96**, 95505.
114 Z. Shuai, H. Geng, W. Xu, Y. Liao and J.-M. André, *Chem. Soc. Rev.*, 2014, **43**, 2662–2679.
115 J. Jiang, K. Liu, W. Lu and Y. Luo, *J. Chem. Phys.*, 2006, **124**, 214711.
116 Y.-H. Shin, I. Grinberg, I.-W. Chen and A. M. Rappe, *Nature*, 2007, **449**, 881–884.
117 A. Jaramillo-Botero, J. Su, A. Qi and W. A. Goddard, *J. Comput. Chem.*, 2011, **32**, 497–512.
118 A. O. Orlov, I. Amlani, G. H. Bernstein, C. S. Lent and G. L. Snider, *Science*, 1997, **277**, 928–930.
119 M. N. Mohammadi and R. Sabbaghi-Nadooshan, *J. Comput. Electron.*, 2015, 1–14.
120 A. Orlov, A. Imre, G. Csaba, L. Ji, W. Porod and G. H. Bernstein, *J. Nanoelectron. Optoelectron.*, 2008, **3**, 55–68.
121 X. Wang, S. Chen, J. Wen and J. Ma, *J. Phys. Chem. C*, 2013, **117**, 1308–1314.

TOC: Simulations using QM and MM methods guide the rational design of functionalized SAMs on surfaces.